A comparative analysis of physical and numerical modelling of debris flow behavior

V. Lentini
University of Enna "Kore", Enna, Italy, valentina.lentini@unikore.it

K.A. Pinargote, E. Basile, F. Castelli
University of Enna "Kore", Enna, Italy, karol.pinargote@phd.unict.it, elisa.basile@unikorestudent.it, francesco.castelli@unikore.it

ABSTRACT: This study presents a comparative analysis between physical and numerical modelling of debris flow behavior with the aim of evaluating the strengths and limitations of each approach in reproducing the mechanisms of slope failure. Physical tests were conducted using a large-scale landslide simulator (LSS), which allows the reproduction of debris flows on an adjustable inclined plane under controlled hydraulic and geometric conditions, conducted at the University of Enna "Kore". The experiments focus on identifying the triggering mechanisms, flow dynamics, and deformation patterns associated with debris movement during progressive water infiltration. At the same time, a numerical model was developed to simulate the same scenarios under equivalent boundary conditions. The simulations incorporate fitting constitutive models to capture the unsaturated behavior of debris material and the evolution of pore water pressure due to rainfall. The comparison between the two approaches is expected to provide valuable insights into the initiation and evolution of debris flows, helping to identify potential consistencies in failure mechanisms and highlight areas where the models may diverge, particularly regarding flow mobility and post-failure behavior. This combined methodology demonstrates the potential of integrating numerical and physical modelling to gain a deeper understanding of debris flow behavior, validate modelling assumptions, and improve the reliability of geotechnical predictions in complex slope environments.

1 INTRODUCTION

Debris flows represent one of the most destructive forms of rapid mass movement, characterized by high velocities, complex rheological behavior, and strong dependence on hydrological conditions (Cruden and Varnes, 1996; Iverson, 1997; Castelli et al., 2018). Their sudden onset and mobility pose significant challenges for hazard assessment and engineering design. While numerical modelling has become a powerful tool for predicting slope instability, its reliability strongly depends on the calibration and validation of constitutive assumptions. Conversely, physical modelling allows direct observation of failure mechanisms but is limited by scaling effects and experimental constraints (Eckersley, 1990; Wang and Sassa, 2001; Lentini et al., 2019).

Within this context, recent research highlights the importance of integrating numerical and physical modelling approaches to better capture the complexity of debris flow processes. This study adopts such an integrated perspective by comparing controlled large-scale physical experiments with numerical simulations reproducing the same boundary and loading conditions. The main aim is to assess the capability of both approaches to capture debris flow initiation, deformation, and post-failure evolution, and to identify their complementary roles in geotechnical engineering applications.

2 PHYSICAL MODELLING OF DEBRIS FLOW

2.1 Experimental apparatus

The experimental activity was carried out using the Large-Scale Landslide Simulator (LSS) installed at the Geotechnics Laboratory of the University of Enna "Kore". The apparatus consists of a rigid flume divided into two main sections, as is illustrated in Figure 1: a triggering channel and an evolution channel. The triggering channel has a length of approximately 1.80 m, while the evolution channel extends for about 3.00 m, resulting in a total flume length close to 4.80 m. The flume width ranges between 0.60 m and 0.65 m, while the sidewalls have a height of approximately 0.70 m, ensuring full confinement of the debris material during testing.

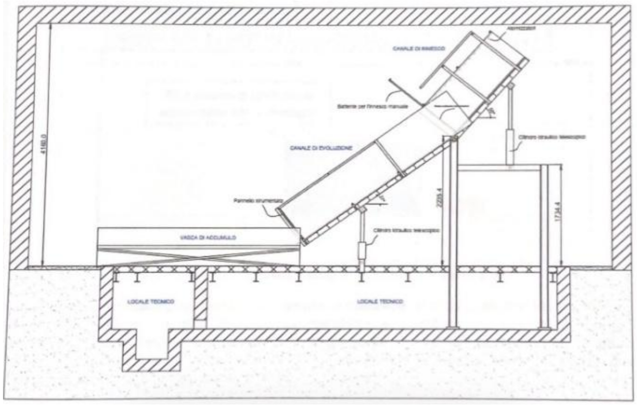

(1)

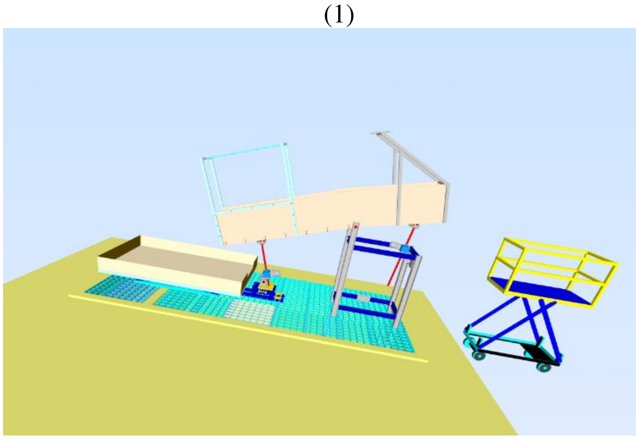

(2)

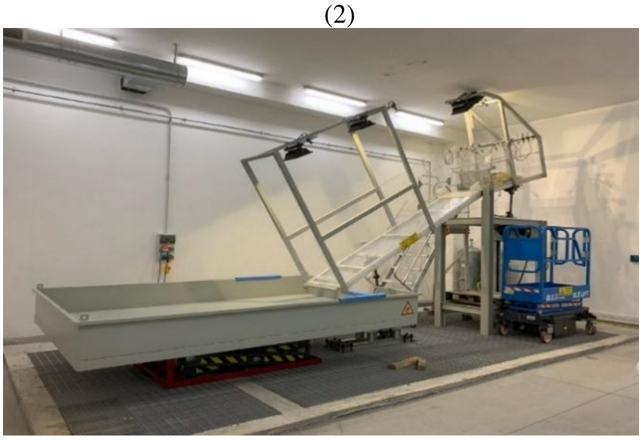

(3)

Figure 1. Overview of the physical modelling setup: (1) lateral view of the physical model; (2) three-dimensional numerical representation of the physical model (lateral perspective); and (3) Large-Scale Landslide Simulator (LSS) installed at the Geotechnics Laboratory of the University of Enna "Kore".

The inclination of the LSS can be adjusted independently for the two sections. In the experimental campaign, the triggering channel inclination ranged between 16° and 20°, while the evolution channel inclination reached values close to 30°. This configuration allowed the reproduction of shallow slope conditions prone to rainfall-induced debris flow initiation and subsequent downslope propagation.

2.2 Material properties and soil preparation

The soil used in the experiments consisted of a reconstituted fine-grained material derived from natural clayey deposits, representative of materials commonly involved in rainfall-induced shallow failures (Fredlund and Rahardjo, 1993). The material was oven-dried, crushed, and sieved to obtain controlled granulometric fractions as is illustrated in Figure 2.

Two main size fractions were selected, corresponding to particles passing the 4.75 mm sieve and those passing the 1.60 mm sieve. These fractions were mixed in predefined proportions to ensure repeatability between tests.

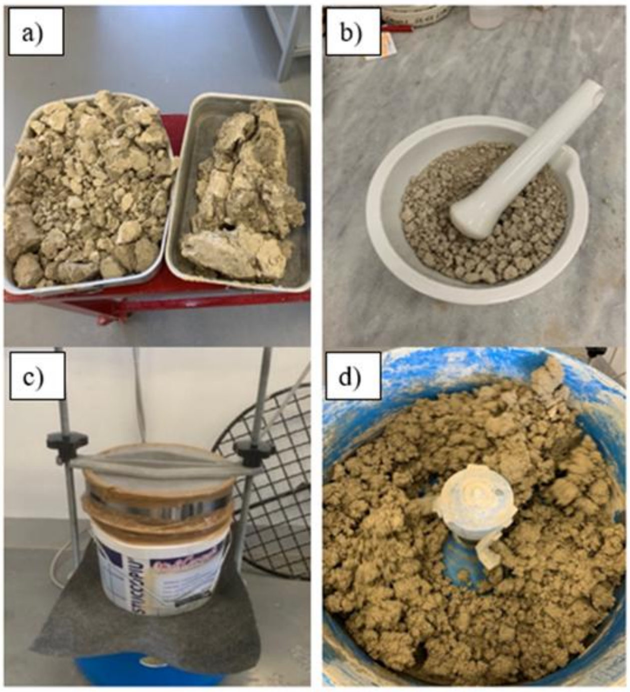

Figure 2. Soil preparation procedure: (a) oven-dried clayey material collected from a borehole; (b) crushing and manual grinding to refine particle size; (c) vibratory sieving with a 1.6 mm mesh; and (d) mechanical mixing of the processed soil.

Water was then added to the dry mixture to reach a target initial water content, and the soil was mechanically mixed using an industrial mixer to obtain a homogeneous paste.

The prepared material was sealed and left to rest for approximately 24 hours to allow uniform moisture redistribution. This procedure ensured reproducible initial conditions and promoted the development of matric suction prior to rainfall application.

2.3 Geotechnical characteristics of the experimental soil

Based on laboratory preparation procedures and typical properties of remoulded clayey soils, the geotechnical parameters adopted to describe the experimental material are summarized in Table 1. These parameters are consistent with values reported in the literature for fine-grained soils subjected to rainfall-induced instability.

Table 1. Geotechnical properties of the experimental soil used in the LSS tests.

Property	Symbol	Range	Unit
Initial water content	ω	17.5-19.6	%
Bulk unit weight (unsat)	γ_{unsat}	16-18	kN/m^3
Bulk unit weight (sat)	γ_{sat}	18-20	kN/m^3
Effective cohesion	c'	1-5	kPa
Effective friction angle	φ'	20-28	°
Young´s modulus	E	2-10	MPa
Poisson´s ratio	ν	0.30-0.35	-

2.4 Instrumentation and monitoring

The experimental setup was equipped with an integrated monitoring system including miniature tensiometers for suction measurements, pore water pressure transducers installed at different depths, displacement sensors to capture surface deformation, and load cells to measure forces at the base of the flume (Figure 3).

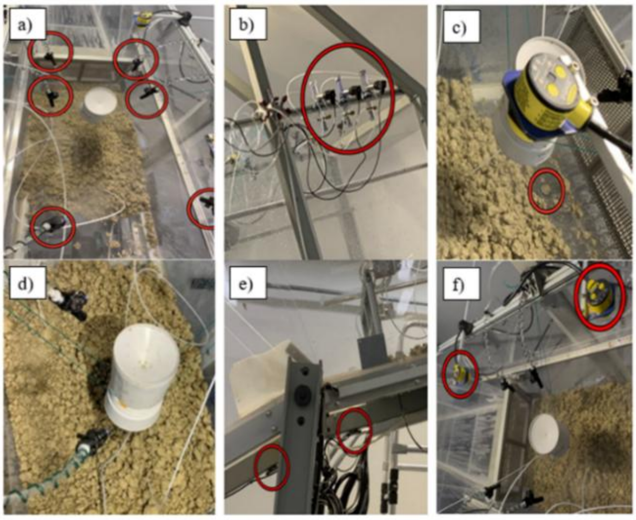

Figure 3. Instrumentation used for the physical simulation: (a) artificial rainfall generation system; (b) tensiometers; (c) pore water pressure transducers; (d) rain gauge; (e) load cells; and (f) displacement sensors.

Rainfall intensity was continuously monitored to ensure consistency with prescribed boundary conditions. Visual observations and image acquisition complemented sensor data, allowing qualitative assessment of deformation patterns and flow evolution.

2.5 Experimental procedure

Two main experimental tests were conducted under comparable geometric and hydraulic conditions. After soil placement and instrumentation, rainfall was applied progressively at constant intensity until instability occurred. The first test lasted approximately 1.5 hours. Due to excessive material weight and insufficient channel inclination, only minor, imperceptible displacements occurred. No debris-flow triggering was observed. The second test was conducted after implementing the improvements identified in Test 1.

Data acquisition was continuous throughout the tests, enabling the identification of precursor phenomena such as suction reduction, progressive deformation, and localized failure zones preceding debris flow initiation as show in Figure 4.

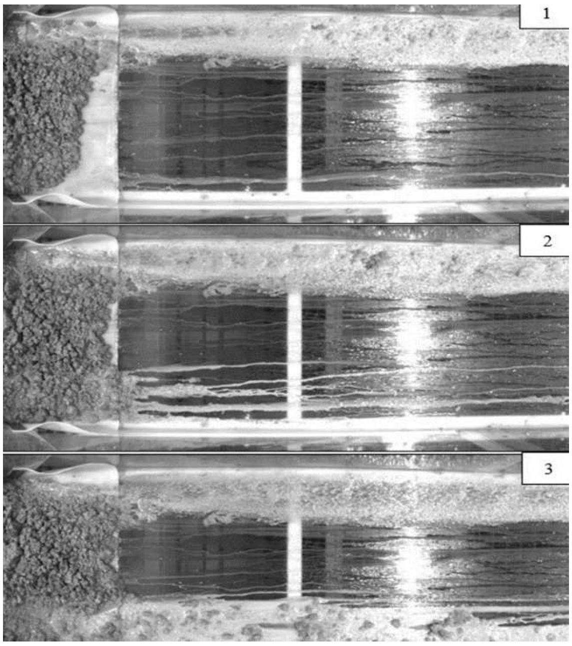

Figure 4. Images acquired by the cameras capturing the propagation phase, during which the viscous flow spreads downslope, forming surface streaks consistent with erosion patterns observed from approximately t ≈ 2457 s onward.

2.6 Experimental results

The experimental results highlighted a progressive failure mechanism controlled by rainfall infiltration, in agreement with laboratory and theoretical studies on debris flow initiation (Iverson, 1997; Wang and Sassa, 2001; Castelli et al., 2016). The experimental results were analyzed by combining displacement measurements obtained from ultrasonic sensors, pore water pressure data recorded by pressure transducers, and rainfall accumulation measured by the rain gauge. Test 2 was therefore selected for numerical comparison, as it represents the reproducible and complete triggering scenario.

2.6.1 Displacement measurements

The ultrasonic sensors (Ultras 1, Ultras 2, and Ultras 3) recorded significant variations in surface elevation during the test, reflecting the progressive deformation and mobilization of the material. At the beginning of the experiment (t = 0 s), the measured displacements were 3.95 mm (Ultras 1), 156.83 mm (Ultras 2), and 60.66 mm (Ultras 3). Prior to failure initiation (t ≈ 2456 s), displacements remained relatively stable, with values of 2.22 mm, 104.12 mm, and 62.94 mm, respectively. After failure and during the propagation phase (t ≈ 3455 s), a marked reduction in measured heights was observed, particularly for Ultras 2 and Ultras 3, which decreased to 42.33 mm and 25.98 mm, indicating rapid material mobilization and erosion (Figure 5).

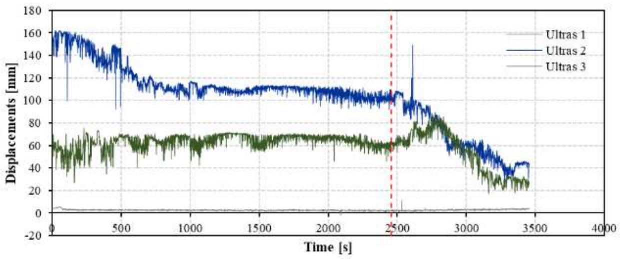

Figure 5. Time histories of ground displacement measured by ultrasonic sensors Ultras 1, Ultras 2, and Ultras 3 during the experiment. The red vertical line indicates the failure initiation time.

These results highlight a transition from a quasi-stable deformation regime to a highly dynamic behavior characterized by rapid changes in surface elevation during flow propagation.

2.6.2 Pore water pressure evolution

The pore water pressure transducers (LM31-1, LM31-2, and LM31-3) provided insight into the hydraulic response of the soil mass. During the pre-failure stage, pore pressures showed limited fluctuations around low positive or slightly negative values, indicating partially saturated conditions.

Approaching the initiation time, a progressive increase in pore water pressure was recorded, followed by abrupt fluctuations immediately after failure (Figure 6).

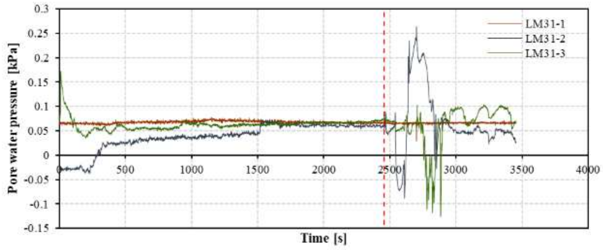

Figure 6. Evolution of pore water pressure recorded by transducers LM31-1, LM31-2, and LM31-3 during the test. The red vertical line marks the onset of debris flow initiation.

The increase in average pore water pressure from the pre- to post-initiation phase suggests a significant reduction in effective stress, consistent with liquefaction-like behavior observed in rainfall-induced debris flows. Rapid oscillations observed after initiation are attributed to internal rearrangement of the material and transient water release during flow propagation, in agreement with observations reported by Wang and Sassa (2001) and Eckersley (1990).

2.6.3 Rainfall accumulation and triggering conditions

Rainfall input was continuously monitored using a rain gauge, allowing the cumulative rainfall volume to be evaluated throughout the experiment. The recorded data show a nearly linear increase in rainfall accumulation until the initiation of failure (*Figure 7*).

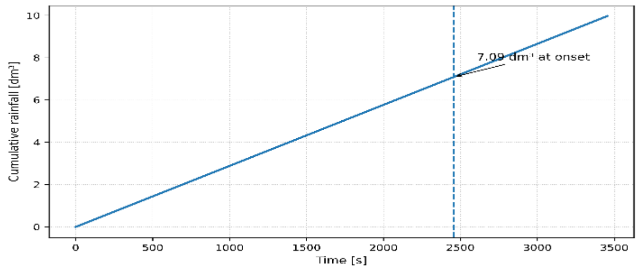

Figure 7. Cumulative rainfall volume measured by the rain gauge during the experiment. The light blue vertical line indicates the failure initiation time.

At the initiation time (t ≈ 2456 s), the accumulated rainfall volume reached approximately 7.5–8.0 dm³, indicating that failure occurred after a critical infiltration threshold was exceeded. This confirms that debris flow initiation was primarily controlled by progressive saturation and pore pressure build-up rather than instantaneous loading.

2.6.4 Integrated interpretation

The combined analysis of displacement and pore water pressure measurements confirms that the observed debris flow exhibited rapid and highly deformable behavior. The increase in pore water pressure led to a reduction in shear resistance, promoting the transition from a stable regime to an unstable, flow-dominated phase, consistent with physical models proposed by Wang and Sassa (2001). Post-initiation, the higher variability observed in both displacement and pore pressure signals indicates a chaotic and less predictable system response, characteristic of active debris flow propagation (Eckersley, 1990).

Overall, the experimental results demonstrate that gradual infiltration governs the pre-failure stage, while post-initiation behavior is dominated by dynamic processes involving erosion, deposition, and internal material rearrangement. These findings provide a robust experimental basis for comparison with numerical simulations.

3 NUMERICAL MODELLING FRAMEWORK

3.1 Numerical approach

The numerical analyses were performed using PLAXIS 2D, adopting a fully coupled hydro-mechanical formulation to simulate rainfall-induced instability in unsaturated soils. This approach allows the interaction between transient seepage and mechanical deformation to be captured consistently, which is essential for reproducing suction loss and pore water pressure build-up during infiltration processes (Fredlund and Rahardjo, 1993; Iverson, 1997).

The numerical model was conceived as a two-dimensional plane strain representation of the Large-Scale Landslide Simulator (LSS), corresponding to the longitudinal section of the experimental flume. Although the lateral confinement imposed by the flume walls cannot be fully reproduced in a 2D framework, this assumption provides a reasonable approximation for analyzing triggering mechanisms and pre-failure deformation patterns.

The model geometry reproduces: Triggering channel length of 1.80 m with a slope of 20°, Evolution channel length of 3.00 m with ~30° (evolution). Finite element discretization was of 15-node triangular elements, global coarseness factor of 1.0, refined mesh along surface and expected shear zone. Typical element size of 0.05 m near surface and 0.10 m in deeper regions.

3.2 Constitutive and hydraulic modelling

The soil was modelled using a Mohr–Coulomb elastoplastic constitutive law under drained conditions, the mechanical parameters adopted are summarized in Table 2, coupled with an unsaturated flow formulation based on the van Genuchten soil-water retention curve, as shown in Table 3. This combination allows simulation of matric suction dissipation and effective stress reduction during rainfall infiltration (Fredlund and Rahardjo, 1993).

Table 2. Mechanical properties to modelled in Plaxis 2D with Mohr-Coulomb.

Property	Symbol	Range	Unit
Unit weight (unsat)	γ_{unsat}	17.5	kN/m^3
Unit weight (sat)	γ_{sat}	19	kN/m^3
Effective cohesion	c'	3	kPa
Effective friction angle	φ'	24	°
Young´s modulus	E	6	MPa
Poisson´s ratio	ν	0.33	-

Hydraulic parameters were calibrated to reproduce the temporal evolution of pore water pressure measured during the experiments. Initial conditions were defined to represent an unsaturated state with negative pore pressures, consistent with laboratory observations.

Table 3. Parameters calculated using the van Genuchten model regarding reproducibility, the full hydraulic parameter.

Property	Symbol	Range	Unit
Saturated permeability	k_{sat}	0.5	m/day
α parameter	α	0.8	$1/m$
Initial suction	ψ_{init}	-10	kPa
Porosity	n_{init}	0.336	-

3.3 Boundary conditions and analysis phases

The basal boundary was assumed to be rigid and impermeable, reflecting the mechanical and hydraulic behavior of the experimental flume. Accordingly, zero horizontal and vertical displacements were prescribed along the base, and a no-flow hydraulic boundary condition was imposed.

The lateral boundaries of the numerical domain were constrained horizontally (u_x=0) while remaining free vertically and were also treated as no-flow boundaries. Rainfall infiltration was simulated by applying a prescribed vertical flux along the upper soil surface in the triggering channel region, reproducing the experimental rainfall intensity and duration.

The numerical analysis was carried out through a sequence of calculation phases. An initial phase was used to establish in-situ stresses and initial suction conditions. Subsequently, a transient infiltration phase was applied by activating the rainfall flux, allowing progressive pore pressure build-up within the soil mass. Finally, a fully coupled phase was used to simulate deformation and identify the onset of instability.

3.4 Modelling results

The outputs of the model included pore pressure distributions during rainfall, hydraulic fields, displacement fields, and global stability curves, which highlighted the progressive development of failure mechanisms within the slope.

3.4.1 Detected displacements

The $|u|$ plot corresponding to the triggering phase reveals a wedge of large displacements developing on the left slope, propagating downslope toward the channel. The red/yellow zone delineates the concentration of the superficial sliding mechanism within the orange soil layer and extends into the yellow–green interface, representing the softer depositional unit (Figure 8). Indicating the development of a sliding mass moving downslope towards the valley.

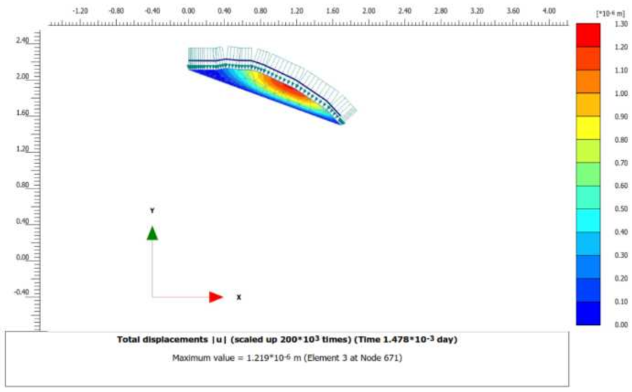

Figure 8. Displacement vectors and failure mechanism identified in the triggering phase. The results highlight the initiation of a rotational–translational landslide on the left slope sector, with maximum deformations concentrated along the inferred failure surface.

3.4.2 Pore pressure and groundwater head evolution

In the Figure 9 the computed field of active pore pressures ($p$active) ranges from -1.00 kPa (at the phreatic surface) down to –3.077 kPa. The presence of suction provides apparent cohesion and temporarily increases soil strength in shallow layers. However, under prolonged rainfall infiltration, suction progressively dissipates, which facilitates the initiation and propagation of slope failure.

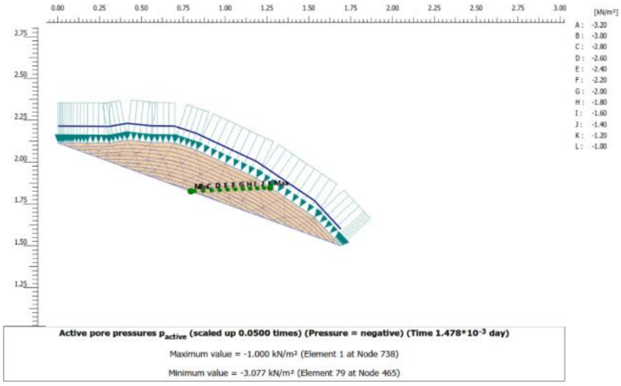

Figure 9. Active pore pressure ($p$active) field illustrating the hydro-mechanical response during infiltration.

In the Figure 10 presents the groundwater head distribution where the calculated hydraulic head field shows maximum values of 2.23 m and minimum values of 1.60 m, highlighting a hydraulic gradient from the upper slope towards the valley bottom. This distribution confirms the presence of recharge in the head area and discharge at the toe, producing elevated pore pressures in deeper regions of the slope. These pore pressures reduce the effective stresses, thereby decreasing the available shear strength of the soil mass.

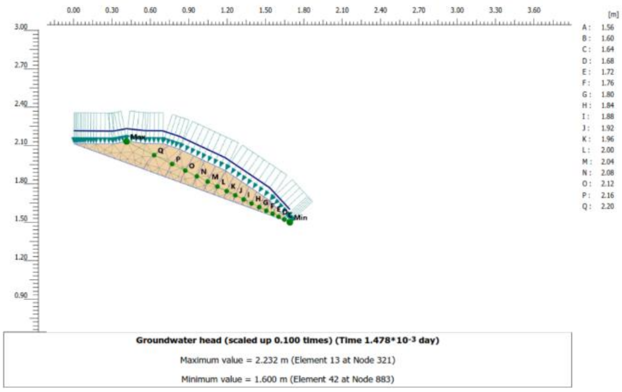

Figure 10. Hydraulic head distribution obtained from the coupled flow–deformation analysis.

4 COMPARATIVE ANALYSIS OF PHYSICAL AND NUMERICAL RESULTS

The comparison between numerical and experimental results focused on key indicators, including time to failure, pore water pressure evolution, and deformation localization. To strengthen the validation of the pore pressure, a point-to-point comparison was performed at sensor location LM31-2 as is shown in Table 4, and also for the displacements at Ultras 2 in Table 5.

Table 4. Measured vs simulated pore pressure at LM31-2 sensor.

Time (s)	Measured (kPa)	Simulated (kPa)
0	-2.8	-2.6
1200	-2.2	-2.1
2000	-1.4	-1.6
2400	-0.6	-0.8
2456 (failure)	-0.1	-0.2

Table 5. Displacement measured at Ultra 2 sensor vs simulated at Plaxis 2D.

Time (s)	Measured (mm)	Simulated (mm)
Pre-failure	104	98
At failure	87	92

The numerical model successfully reproduced the progressive suction reduction, timing of near-zero pore pressure, delay between rainfall and instability.

The model captures the progressive deformation, localized shear band formation and similar failure surface geometry.

4.1 Limitations of the Numerical Approach

Despite the satisfactory agreement obtained between experimental observations and numerical simulations, several limitations of the adopted modelling approach should be acknowledged. The soil behaviour was simulated using the Mohr–Coulomb constitutive model, which assumes perfectly plastic behaviour and does not capture strain-softening, progressive failure mechanisms, or post-peak strength reduction that may occur during debris-flow initiation. The hydraulic response in the unsaturated zone was modelled using calibrated retention and permeability functions; however, uncertainties in van Genuchten parameters and initial suction distribution may influence the timing and magnitude of pore-pressure build-up.

5 CONCLUSIONS

The comparative analysis between physical and numerical modelling presented in this study highlights the capability of large-scale laboratory tests to capture key mechanisms governing rainfall-induced debris flow initiation. The experimental results clearly show that progressive infiltration leads to a reduction of matric suction, followed by pore water pressure build-up and strain localization, ultimately triggering rapid mass mobilization. These processes were consistently identified through direct measurements, confirming the suitability of the LSS for reproducing shallow debris flow phenomena under controlled conditions.

The numerical simulations implemented using a fully coupled flow–deformation formulation with explicitly defined mechanical and hydraulic parameters, including permeability, water retention behavior, and initial suction distribution, successfully reproduced the temporal evolution of pore pressure and the onset of instability observed experimentally.

Overall, the study demonstrates that physical modelling provides essential insight into triggering mechanisms and early-stage deformation, while numerical modelling offers a rigorous framework for interpreting hydraulic–mechanical coupling and performing parametric investigations. Their combined application enhances model calibration, improves the quantitative interpretation of experimental data, and increases the reliability of geotechnical assessments for slopes susceptible to rainfall-induced debris flows.

ACKNOWLEDGEMENTS

This study was carried out within the RETURN Extended Partnership and received funding from the European Union Next-GenerationEU (National Recovery and Resilience Plan – NRRP, Mission 4, Component 2, Investment 1.3 – D.D. 1243 2/8/2022, PE0000005).

REFERENCES

Castelli, F., Maugeri, M. and Lentini, V. (2016). Experimental analysis of rainfall-induced shallow landslides. Engineering Geology, 206, pp. 28–39.

Castelli, F., Maugeri, M. and Lentini, V. (2018). Physical modelling of debris flow initiation in unsaturated granular soils. Geotechnical and Geological Engineering, 36(5), pp. 2981–2996.

Cruden, D.M. and Varnes, D.J. (1996). Landslide types and processes. In: Landslides: Investigation and Mitigation, Special Report 247, Transportation Research Board, National Academy Press, Washington, D.C., pp. 36–75.

Eckersley, J.D. (1990). Instrumented laboratory flowslides. Géotechnique, 40(3), pp. 489–502.

Fredlund, D.G. and Rahardjo, H. (1993). Soil Mechanics for Unsaturated Soils. John Wiley & Sons, New York.

Iverson, R.M. (1997). The physics of debris flows. Reviews of Geophysics, 35(3), pp. 245–296.

Lentini, V., Castelli, F. and Maugeri, M. (2019). Laboratory investigation on rainfall-induced instability of shallow deposits. Soils and Foundations, 59(4), pp. 1023–1036.

Okura, Y., Kitahara, H., Sammori, T. and Kawanami, A. (2002). The effects of rockfall volume on runout distance. Engineering Geology, 67(3–4), pp. 243–254.

Wang, G. and Sassa, K. (2001). Factors affecting rainfall-induced flowslides in laboratory flume tests. Géotechnique, 51(7), pp. 587–599.